Rapid Prototyping of an Electrically-Small Antenna for Binaural-Hearing Instruments

Andrea Ruaro*†, Jesper Thaysen*, and Kaj B. Jakobsen†

*GN ReSound A/S, Lautrupbjerg 7, DK-2750 Ballerup, Denmark
†Department of Electrical Engineering, Technical University of Denmark, DK-2800 Lyngby, Denmark

***Abstract*—Rapid prototyping is emerging as a technology that can provide detailed mechanical parts, e.g., for use in antenna mock-ups, in a short lead time. Nevertheless, one of the main issues associated with it is that the materials suitable for 3D printing are not characterized at radio frequencies (RF). This study analyzes the main RF parameters (dielectric constant, loss tangent, surface roughness) and applies the results to the modeling of the prototype of an electrically small (ESA) antenna for binaural hearing instruments applications. After discussing the specific technology choices and their relevancies, it is shown how the analyzed parameters can be used to obtain good correlation between simulations and measurements.**

***Index Terms*—Rapid prototyping; electrically small antennas (ESA); wireless body-area networks (WBAN); electromagnetic compatibility (EMC); consumer electronics.**

I. Introduction

Rapid prototyping in the electronics industry is of special interest due to the possibility to have access to prototypes at a very early stage, i.e., as soon as the mechanical design is outlined. Rapid prototyping, also known as 3D printing, is emerging today as a technology that enables fast fabrication of devices. The printed devices are typically inexpensive and easy-to-build. The technology has been used, e.g., for antenna prototypes and to manufacture a 60 GHz plastic lens-antenna [1]–[3]. For the antenna designer, this translates into a great potential of building mechanical support for its designs. On the other side, the performance of the evaluation mock-ups is extremely dependent upon the process itself. The ability to identify and separate the critical factors from the non-critical is important in order to be able to model the antennas in an efficient way.

RF and antenna electronics poses serious challenges on 3D printed prototypes. In fact, even though the freedom during the design process is a great advantage for the engineering of the device, the material itself strongly impacts the result. In particular, it is necessary to establish a correlation among the 3D-printed prototype and the final parts that will be used in the mass production. In fact, specific deposition processes for the conductive parts have to be studied. The main issue, nevertheless, is with the electrical properties of the plastics themselves. Some processes may prove to be better than others in this regard, but this still has to be studied. Among the potential issues there are: the inclusion of air bubbles within the plastics that changes the effective dielectric constant from prototype to prototype, or from batch to batch; inherently higher loss tangent as compared to cast plastic; poor or non-existing RF characterization of the materials.

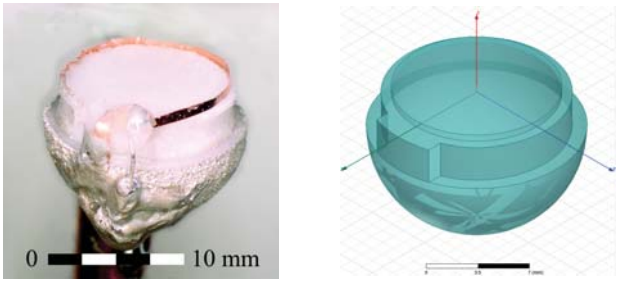

(a) (b)

Fig. 1: Photo of the prototype (a) and rendering of the 3D-printed mechanical support (b), respectively.

Nevertheless, the understanding and correct modeling of such properties would allow the antenna designers to evaluate their prototypes. As an application example, in the hearing instruments (HI) there is a need to wirelessly connect two devices placed at each ear with an ear-to-ear (E2E) link, as this allows for more advanced signal processing [4]. Recently, a few solutions have been proposed by different authors [5]–[8]. The 2.4 GHz ISM band is preferred here due to its world-wide availability and the amount of available communications standards, such as Bluetooth Low Energy (BLE) or ZigBee. In this study, Selective Heat Sintering (SHS) 3D-printed plastics are used as the frame of an antenna for binaural hearing instruments.

The article is organized as follows: Section II describes the antenna design and implementation. In the following section, the main electrical parameters are analyzed. Section IV then presents and discusses the simulation and measurement results. Finally, Section V summarizes the findings.

II. Antenna Design and Implementation

The prototype antenna comprises of an Inverted-F Antenna (IFA) arm, bent on a plane situated above an hemispherical ground plane with a radius of $r = 7.5$ mm. This concept was recently introduced for on-body devices, and it is suitable for the use in binaural hearing instruments due to its good radiation efficiency and polarization characteristic [9], [10]. The electrical size of the antenna at 2.4 GHz is $ka = 0.38$,

where k is the free space propagation constant, and a the radius of the sphere circumscribing the antenna. Thus the antenna can be contained within the Wheeler radiansphere [11] since the electrical length is less than one radian, i.e., it is an electrically small antenna [12].

A picture of the antenna is shown in Fig. 1a. A more substantial description of the antenna is found in [9].

The mechanical support for the antenna, shown in Fig. 1b, is prototyped with additive manufacturing. A SHS 3D printer is used to build the frame. In this technology, moderate heat is selectively applied to a thin layer of a specific thermoplastic powder in order to bind it together and to form a solid structure. The process is repeated after the deposition of a new layer until the desired height is reached.

The hemispherical ground plane is then metalized with conductive paint. The feed structure is electrically connected with conductive glue. If soldering is preferred, since the heat produced during the soldering process can damage the plastic support, it is possible to solder the feed structure on a thin layer of solid copper and afterwards connect or couple it to the ground plane. The IFA arm is made of solid copper with an electrical conductivity of $58 \cdot 10^8$ S/m.

III. Parameter Analysis

A. Surface Roughness

The ability to custom shape the mechanical frame by the 3D printing process on one hand gives multiple advantages, but on the other hand the printing process challenges other aspects of the prototype. E.g., in this case, where a hemispherical ground plane needs to have a good conductivity, different layers of a polycrystalline conductive paint are applied to the antenna support. The porosity of the 3D printed plastics causes it to be partly absorbed into the frame. This results in a complicated profile that is hard to inspect and model. If the roughness of the deposited metal layer by the fabrication method is significant, the recently-developed Huray loss model can be used [13].

In the present work, the results show that an accurate model for the metal surface roughness ρ_{s} is not necessary in order to achieve good agreement between the simulations and measurements.

B. Dielectric Constant

The dielectric constant plays a fundamental role in every simulation model. In fact, parameters like the electrical length of an antenna on a substrate depends significantly on the effective dielectric constant $\varepsilon_{\mathrm{eff}}$ that is mostly determined by the material properties. Unfortunately, such value is not provided by the 3D printer manufacturers: mainly, it falls out of their main scope. Furthermore, in a fast-growing and competitive business as that of 3D printing, it seems to be normal that the manufacturers do not want to disclose specific information about the printing material, as it is part of their competitive advantage. In Table I the relative permittivity values of the mean μ and the standard deviation σ for a set of cast, stereolithography (SLA), and SHS plastics at 2.4 GHz are reported. The results are mostly indicative and were obtained by the use of the cavity perturbation method, where a sample is inserted into a resonant cavity and its properties are inferred from the resulting variation in resonant frequency and bandwidth. Injection molding is a technique traditionally not used in the evaluation of prototypes, as it is the method most often used in the final production. RF-wise, they exhibit higher density and lower losses as compared to the plastics obtainable with 3D printing processes. The SHS process shows the lowest $\varepsilon'_{\mathrm{r}}$, i.e., the largest deviation from the solid plastic properties. The other 3D-printing process analyzed here is a modified SLA that uses a liquid photo-polymer resin that is cured layer-by-layer by an ultraviolet laser to selectively solidify the pattern. The SLA and cast plastics data are here presented in an aggregated form. The higher variance for the first two cases depends on the size of the test population, that is much larger and varies more than in the third case.

TABLE I: Mean and standard deviation, $\mu \pm \sigma$, for the relative permittivity and loss tangent at 2.4 GHz for cast (injection molded), SLA, and SHS plastic

Process	$\varepsilon'_{\mathrm{r}}$	$\tan\delta$
Cast	2.8 ± 0.2	0.006 ± 0.002
SLA	2.53 ± 0.03	0.024 ± 0.005
SHS	2.40 ± 0.01	0.012 ± 0.0006

C. Loss Tangent

Dielectric losses plays a crucial role as well. In fact, it is shown here that this by far is the largest contribution to the overall losses. It is observed that it is possible to obtain good agreement between simulations and measurements when the conductive losses are neglected. The loss tangent $\tan\delta$ was estimated by the use of the cavity perturbation method as well and are shown in Table I.

The loss tangent is a critical parameter since the measured Total Radiated Power (*TRP*) depends nearly entirely on it. The *TRP* performance is a key parameter when the prototype designs are to be evaluated in the early stage. If the loss mechanism in not well understood, the result could be that a decision is made for an over- or underestimated design.

In particular, the SLA process exhibits particularly high losses. This complicates the evaluation scenario for mock-ups. The SHS process shows instead contained losses—about twice that of cast plastics and half of those obtainable by SLA.

IV. Measurement Results and Discussion

The characterization is done in terms of the antenna total radiation efficiency η_{tot}, i.e., a function of two important parameters: the reflection coefficient Γ at the antenna input terminals and the antenna radiation efficiency η_{rad} and is given by

$$\eta_{\mathrm{tot}} = (1 - |\Gamma|^2)\ \eta_{\mathrm{rad}}\ . \tag{1}$$

The total radiation efficiency η_{tot} is obtained by measurement of the total radiated power *TRP* in a radio anechoic chamber.

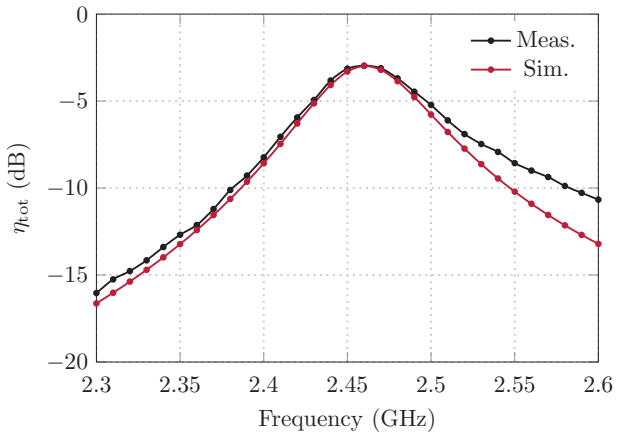

Fig. 2: Measured (black line) and simulated (red line) total radiation efficiency, η_{tot}.

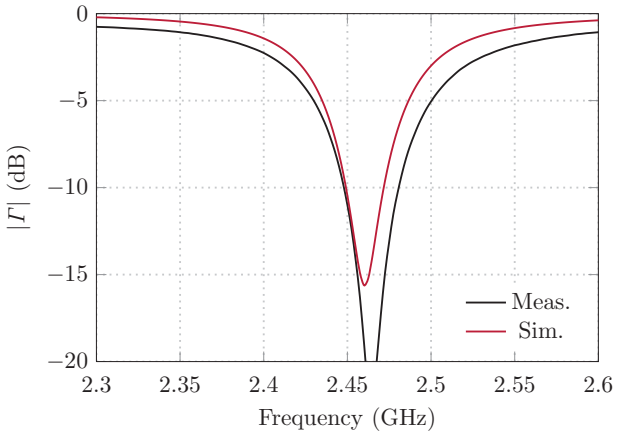

Fig. 3: Measured (black line) and simulated (red line) reflection coefficient at the antenna terminals, $|\Gamma|$.

Since the antenna is well impedance matched, $|\Gamma|^2 \approx 0$ at the center frequency. Hence, the total radiated efficiency is approximately equal to *TRP* normalized with respect to the input power. In order to measure the reflection coefficient Γ at the true antenna terminals, a Vector Network Analyzer (VNA) with a corrected port extension has been used. The simulations are run with a FEM solver (Ansys HFSS®). All simulations and measurements are conducted in free space.

The total radiation efficiency is shown in Fig. 2, whereas the reflection coefficient is reported in Fig. 3. There is an excellent agreement among the simulated (red line) and measured (black line) antenna total efficiency. This is supportive of the fact that the main loss mechanism is not linked to the skin effect on the conductor, but to the dielectric losses in the plastic frame. The efficiency falls in the high range for the purpose of the application in practical HI. The deviation between the curves above the higher band edge is likely due to spurious currents, as the used balun is inherently narrowband. The potential radiation efficiency varies slowly with respect to the frequency.

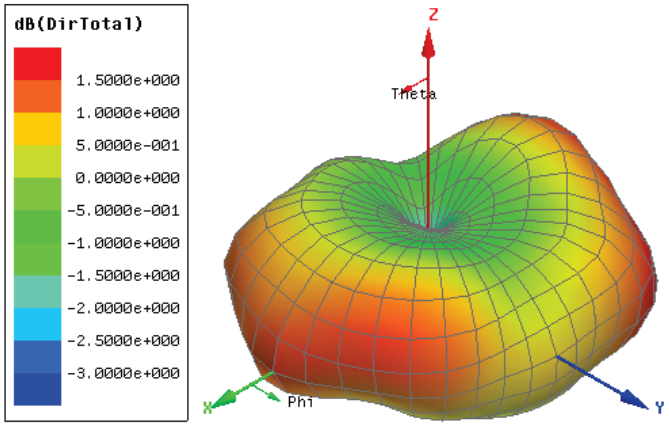

Fig. 4: Simulated directivity (in dB) of the antenna.

The matching provided by the shorting pin of the IFA sets the actual bandwidth. The 3D radiation pattern of the antenna is shown in Fig. 4, where the antenna is oriented as in Fig. 1.

V. Conclusion

The material properties of 3D-printed plastics have been characterized. This allows for efficient and accurate modeling of an antenna for binaural hearing instruments. A SHS printer was used to manufacture the antenna frames. The plastic properties were assessed by the cavity perturbation method. The conductive losses have been analyzed. It was discovered that they had insignificant influence in this application.

An electrically small wearable antenna suitable for E2E communications was implemented and modeled. Excellent agreement between simulations and measurements was obtained. To conclude, it is possible to use rapid prototyping for mock-ups, given that the electrical properties are known.

VI. Acknowledgements

The authors would like to thank Dr. Gianluca Fabio Dorini of Blueprinter A/S for the support and valuable discussions, in addition to sourcing the 3D-printed parts.

References

[1] J. Tribe, W. G. Whittow, R. W. Kay, and J. C. Vardaxoglou, "Additively manufactured heterogeneous substrates for three-dimensional control of local permittivity," *Electronics Letters*, vol. 50, no. 10, pp. 745–746, 2014.

[2] O. S. Kim, "Rapid prototyping of electrically small spherical wire antennas," *IEEE Transactions on Antennas and Propagation*, vol. 62, no. 7, pp. 3839–3842, 2014.

[3] A. Bisognin, D. Titz, F. Ferrero, R. Pilard, C. A. Fernandes, J. R. Costa, C. Corre, P. Calascibetta, J.-M. Riviere, A. Poulain, C. Badard, F. Gianesello, C. Luxey, P. Busson, D. Gloria, and D. Belot, "3D printed plastic 60 GHz lens: Enabling innovative millimeter wave antenna solution and system," *IEEE MTT-S International Microwave Symposium Digest*, 2014.

[4] B. C. Kirkwood, S. A. Hallenbeck, and T. Stender, "How can wireless data exchange in hearing instruments contribute to binaural hearing?" *Hearing Review*, vol. 19, no. 10, pp. 52–55, 2012.

[5] N. Kammersgaard, S. Kvist, J. Thaysen, and K. Jakobsen, "In-the-ear spiral monopole antenna for hearing instruments," *Electronics Letters*, vol. 50, no. 21, pp. 1509–1511, October 2014.

[6] R. Chandra and A. J. Johansson, "A link loss model for the on-body propagation channel for binaural hearing aids," *IEEE Transactions on Antennas and Propagation*, vol. 61, no. 12, pp. 6180–6190, 2013.

[7] L. Huitema, S. Sufyar, C. Delaveaud, and R. D'Errico, "Miniature antenna effect on the ear-to-ear radio channel characteristics," *Proceedings of 6th European Conference on Antennas and Propagation (EuCAP 2012)*, pp. 3402–3406, 2012.

[8] W. H. Yatman, L. K. Larsen, S. H. Kvist, J. Thaysen, and K. B. Jakobsen, "In-the-ear hearing-instrument antenna for ISM-band body-centric ear-to-ear communications," *2012 Loughborough Antennas and Propagation Conference (LAPC)*, 2012.

[9] A. Ruaro, J. Thaysen, and K. B. Jakobsen, "Cavity-backed on-body antenna for custom hearing instrument applications," *accepted to Electronics Letters*, 2015.

[10] S. H. Kvist, S. Özden, J. Thaysen, and K. B. Jakobsen, "Improvement of the ear-to-ear path gain at 2.45 GHz using parasitic antenna element," *6th European Conference on Antennas and Propagation*, vol. 2, pp. 944–947, 2011.

[11] H. Wheeler, "The radiansphere around a small antenna," *Proceedings of the Institute of Radio Engineers*, vol. 47, no. 8, pp. 1325–1331, 1959.

[12] ——, "Fundamental limitations of small antennas," *Proceedings of the Institute of Radio Engineers*, vol. 35, pp. 1479–1484, 1947.

[13] P. G. Huray, O. Oluwafemi, J. Loyer, X. Ye, and E. Bogatin, "Impact of copper surface texture on loss: A model that works," *DesignCon 2010*, vol. 1, pp. 462–483, 2010.